Journal of Computational Physics 229 (2010) 2425–2431

Contents lists available at ScienceDirect

Journal of Computational Physics

journal homepage: www.elsevier.com/locate/jcp

Short Note

A Fourier-based elliptic solver for vortical flows with periodic and unbounded directions

Philippe Chatelain *, Petros Koumoutsakos

Chair of Computational Science, ETH Zurich, CH-8092 Zurich, Switzerland

ARTICLE INFO

Article history:
Received 1 August 2009
Received in revised form 11 December 2009
Accepted 30 December 2009
Available online 11 January 2010

Keywords:
Elliptic solver
Unbounded domain
Infinite domain
Particle methods
Vortex methods

ABSTRACT

We present a computationally efficient, adaptive solver for the solution of the Poisson and Helmholtz equation used in flow simulations in domains with combinations of unbounded and periodic directions. The method relies on using FFTs on an extended domain and it is based on the method proposed by Hockney and Eastwood for plasma simulations. The method is well-suited to problems with dynamically growing domains and in particular flow simulations using vortex particle methods. The efficiency of the method is demonstrated in simulations of trailing vortices.

1. Introduction

Simulations of flows such as jets and wakes require an unbounded computational domain. Periodic domains are however usually employed to take advantage of available FFT-based elliptic solvers for the solution of the associated Poisson equation. It has been demonstrated [8] that the use of periodic or unbounded domains can affect the dynamics of the flow. The straightforward approach of employing large periodic boxes to alleviate the effects of the periodic images, requires in turn large numbers of computational elements that almost void the benefits of using fast elliptic solvers.

Hybrid techniques have been developed that balance the requirement for computational efficiency with the geometric requirements of the flow, by combining domains that are unbounded in one or two dimensions while maintaining periodicity in the other dimensions. In [9] a cartesian and a cylindrical mesh are coupled and the method relies on an analytical representation of the velocity field in order to match solutions in the periodic and the unbounded parts of the domain. The method is well-suited for simulations of vortical flows such as aircraft wakes. In [11] unbounded–periodic simulations are performed using vortex methods using images of the vorticity field to account for periodicity, thus allowing for a seamless integration of the periodic and unbounded domains in a Fast Multipole summation algorithm. A set of successively coarser grids is implemented in [3] to solve the Poisson equation with Dirichlet boundary conditions in each grid thus emulating zero far-field conditions for bluff body flows.

The use of periodic domains in lieu of nominally unbounded domains for the solution of elliptic problems is not unique to fluid mechanics. Hockney and Eastwood [5], hereafter referred to as HE, have proposed more than 30 years ago a method that operates on the wave space to perform the convolutions necessary for solving the Poisson equation in unbounded domains. In this paper, we extend this method and combine it with adaptive particle methods so as to simulate flows in

* Corresponding author. Present address: Department of Mechanical Engineering, Louvain School of Engineering, Université Catholique de Louvain, B-1348 Louvain-la-Neuve, Belgium.

E-mail addresses: philippe.chatelain@uclouvain.be (P. Chatelain), petros@ethz.ch (P. Koumoutsakos).

0021-9991/$ - see front matter © 2010 Elsevier Inc. All rights reserved.
doi:10.1016/j.jcp.2009.12.035

periodic–unbounded domains. The method relies on FFTs in all directions for the solution of the elliptic problem at the cost of doubling the domain size in the non-periodic directions. The use of FFTs enables the straightforward implementation of this technique with existing Fourier-based Poisson solvers.

This paper is organized as follows. Section 2 presents the elliptic solver for unbounded and mixed periodic–unbounded geometries, the vortex particle method and its implementation. In Section 3, we apply this approach to vortical instabilities

2. Methodology

The focus of this work is the solution of the Poisson equation for flow simulations in remeshed vortex methods [6]. We introduce however the methodology using the Helmholtz equation as it readily reduces to the Poisson equation and as it is the governing equation in cases where the elliptic problem is solved with one or two periodic directions. The Helmholtz equation reads

$$\Delta u + \lambda^2 u = -f \tag{1}$$

in an unbounded domain $\mathbb{R}^d$ $(d = 2, 3)$, or a domain with one or two periodic directions $\mathbb{R}^d/\mathbb{Z}^{d'}$ $(d' = 1, 2)$.

The solution of this equation can be expressed as a convolution $(u(\mathbf{x}) = G_\lambda \star f(\mathbf{x}))$ with the fundamental solution of the equation G_λ. For unbounded domains in two and three dimensions, these functions are given by

$$G_\lambda^{2D}(\mathbf{x}) = \frac{i}{4} H_0^{(1)}(\lambda|\mathbf{x}|), \quad G_\lambda^{3D}(\mathbf{x}) = \frac{e^{i\lambda|\mathbf{x}|}}{4\pi|\mathbf{x}|} \tag{2}$$

where $H_0^{(1)}$ is the Hankel function of the first kind. The convolution can be carried out in real space by means of fast summation algorithms such as Fast Multipole Methods [4,2]. FMM respect the unbounded domain but their computational implementation lags well behind the implementation of FFTs. In turn FFTs imply a periodic domain but as has been proposed in [5], a simple extension of the domain can emulate an unbounded domain albeit at doubling the cost of the solver for each unbounded direction.

2.1. A Fourier solver for unbounded domains

The algorithm proposed by HE for solving the Poisson equation in unbounded domains using FFTs involves two steps

(1) Double the original domain of definition of the right-hand side f and pad the extension with zeros. The zero padding eliminates the effects of the periodic images.
(2) Solve the Helmholtz equation in wave space (for the extended domain): $\hat{u}(\mathbf{k}) = \widehat{G}_\lambda(\mathbf{k})\hat{f}(\mathbf{k})$. The upper halves of the result of the inverse transforms are discarded.

The transform of the fundamental solution $\widehat{G}_\lambda$ only has to be computed once and stored. In three dimensions, the fundamental solution G_λ is initialized on the extended domain $(2N_X \times 2N_y \times 2N_z)$, the extension being even images of G_λ

$$G_{i,j,k} = \begin{cases} G^{3D}(i\Delta x, j\Delta y, k\Delta z) & \text{if } i \leqslant N_x,\ j \leqslant N_y,\ k \leqslant Nz \\ G^{3D}((2N_x - i)\Delta x, j\Delta y, k\Delta z) & \text{if } i > N_x,\ j \leqslant N_y,\ k \leqslant Nz \\ G^{3D}(i\Delta x, (2N_y - j)\Delta y, k\Delta z) & \text{if } i \leqslant N_x,\ j \leqslant N_y,\ k \leqslant Nz \\ \ldots \end{cases} \tag{3}$$

The singularity at (0,0,0) is integrable and is replaced with its average contribution in a cell volume. A simple analytical expression is obtained by substituting a spherical volume equivalent to the cubic cell

$$G_{0,0,0} = \int_{-\Delta x/2}^{\Delta x/2} \int_{-\Delta y/2}^{\Delta y/2} \int_{-\Delta z/2}^{\Delta z/2} G^{3D}(x, y, z)\, dx\, dy\, dz \tag{4}$$

$$\simeq \int_0^{\pi} \int_{-\pi}^{\pi} \int_0^{r_{eq}} \frac{e^{i\lambda r}}{4\pi r} \sin(\psi) r^2\, dr\, d\theta\, d\psi \simeq \frac{(1 - i\lambda r_{eq})e^{i\lambda r_{eq}} - 1}{\lambda^2} \tag{5}$$

where $r_{eq} = \sqrt[3]{\frac{3\Delta x \Delta y \Delta z}{4\pi}}$. In the case $\lambda = 0$, the above expression reduces to $r_{eq}^2/2$. The initialization is completed by the forward transform of $G_{i,j,k}$ and its storage.

2.2. A periodic–unbounded solver

We extend the algorithm of HE to the case of mixed periodic–unbounded conditions. This requires the additional step of splitting the Laplacian operator according to the periodic and unbounded directions. In three dimensions with periodicity in the z-direction we write

$$\Delta_{xy}u + \frac{\partial^2 u}{\partial z^2} + \lambda^2 u = -f \quad (6)$$

A Fourier transform in the periodic direction yields

$$\Delta_{xy}\tilde{u} + \left(\lambda^2 - k_z^2\right)\tilde{u} = -\tilde{f} \quad (7)$$

where we define $\tilde{u}(x, y, k_z)$ as the z-transformed field.

For a given k_z, this is a two-dimensional unbounded Helmholtz equation. The approach discussed in Section 2.1 for two unbounded directions thus applies. For every constant-k_z plane, the fundamental solution of Eq. (7) is

$$G^{2D}_{\sqrt{\lambda^2-k_z^2}}(x,y) = \frac{i}{4}H_0^{(1)}\left(\left(\lambda^2 - k_z^2\right)^{1/2}\sqrt{x^2+y^2}\right) \quad (8)$$

Because we focus on a fluid simulation application, we detail the case of the Poisson equation ($\lambda = 0$). The expression above then involves an imaginary parameter for all $k_z > 0$ and becomes

$$G^{2D}_{i|k_z|}(x,y) = \begin{cases} \frac{1}{2\pi}\ln\left(\sqrt{x^2+y^2}\right) & \text{if } k_z = 0 \\ \frac{1}{2\pi}K_0(|k_z|(\sqrt{x^2+y^2})) & \text{otherwise} \end{cases} \quad (9)$$

This expression is singular at $(x, y) = (0, 0)$. We regularize it with the average cell value, which yields

$$G^{2D}_{i=0,j=0,k_z} = \begin{cases} \frac{2\ln\left(1+\sqrt{2}\right)}{\pi^{3/2}r_{eq}^{2D}} & \text{if } k_z = 0 \\ \frac{1-k_z r_{eq}^{2D}K_1\left(k_z r_{eq}^{2D}\right)}{\pi\left(k_z r_{eq}^{2D}\right)^2} & \text{otherwise} \end{cases} \quad (10)$$

The initialization and solution steps are then similar to the all-unbounded case. We note that the extension to the general case $\lambda \neq 0$ is immediate.

Let us mention finally the cases of two dimensions with one periodic direction (y) and three dimensions with two periodic directions (y and z). They can be treated in a similar fashion and involve the fundamental solution of the Helmholtz equation in one dimension

$$G^{1D}_{\sqrt{\lambda^2-k_y^2(-k_z^2)}}(x) = \frac{i\,e^{i\sqrt{\lambda^2-k_y^2(-k_z^2)}x}}{2\sqrt{\lambda^2-k_y^2(-k_z^2)}} \quad (11)$$

2.3. Vortex particle method

We consider a three-dimensional incompressible flow and the Navier–Stokes equations in their velocity ($\mathbf{u}$)-vorticity ($\boldsymbol{\omega} = \nabla \times \mathbf{u}$) form

$$\frac{D\boldsymbol{\omega}}{Dt} = (\boldsymbol{\omega}\cdot\nabla)\mathbf{u} + \nu\nabla^2\boldsymbol{\omega} \quad (12)$$

$$\nabla \cdot \mathbf{u} = 0 \quad (13)$$

where $\frac{D}{Dt} = \frac{\partial}{\partial t} + \mathbf{u}\cdot\nabla$ denotes the Lagrangian derivative and ν is the kinematic viscosity. The velocity field is the solution of the Poisson equation

$$\nabla^2\mathbf{u} = -\nabla \times \boldsymbol{\omega} \quad (14)$$

The vorticity field is discretized by particles, characterized by a position $\mathbf{x}_p$, a volume V_p and a strength $\boldsymbol{\alpha}_p = \int_{V_p}\boldsymbol{\omega}\,d\mathbf{x}$. Particles are convected by the flow field and their strengths are modified according to Eq. (12). We use a hybrid method where the velocity field and the right-hand side differential operators are first computed on the mesh through the use of Fast Poisson solvers and Finite Differences. The results of these calculations on the grid are then interpolated back onto the particles. We refer to [1] for an extensive description of the method and its implementation for large parallel architectures.

2.4. Discussion

The implementation of our extension to the HE technique is immediate for an existing FFT-based solver. The only additional precautions concern the padding of the domain and the preliminary computation of the transformed Green's function.

The costs incurred in this technique are twofold. Storage will have to accommodate the precomputed Green's function and a wavespace field which has doubled in size for each unbounded direction. We note that this overhead can be alleviated through straightforward optimizations: the symmetries of the Green's function can be exploited and by choosing an unbounded direction for the innermost transform, one can combine the forward transform, the product and the inverse transform.

The computational overhead will depend on the aspect ratio of the geometry, i.e. the unbounded dimensions with respect to the periodic ones; for two unbounded directions and a cubic geometry, the overhead factor will be of approximately 2.5.

Finally, the present approach allows the computational domain to grow or shrink according to the support of the right-hand side of the PDE, a step which is facilitated by our use of a particle method. A threshold is necessary to make this growth practicable: vorticity below this threshold is allowed to exit the domain but vorticity above that threshold in the neighborhood of boundaries triggers a domain growth. Conversely, the absence of significant vorticity near the computational boundaries allows us to shrink the domain.

This truncation technique entails an approximation as it corresponds to a vorticity sink term in a modified vorticity transport equation. The intensity of this sink term and the distance between its support and the physics of interest are controlled by the threshold value. We underline two consequences. This term is not necessarily divergence-free, thus potentially generating vorticity with $\nabla \cdot \boldsymbol{\omega} \neq 0$. Over time, this approach can also lead to large computational domains, in particular if slowly decaying structures advect to large distances. This happens, to a limited extent, in the examples of Section 3 where the initial problem size is small enough to use a restrictive, i.e. small, threshold. We mention two possible solutions that would rely on coarsening of the grid

(1) over time: the mesh resolution can be uniformly decreased for problems which are developing spatially but decaying over time;

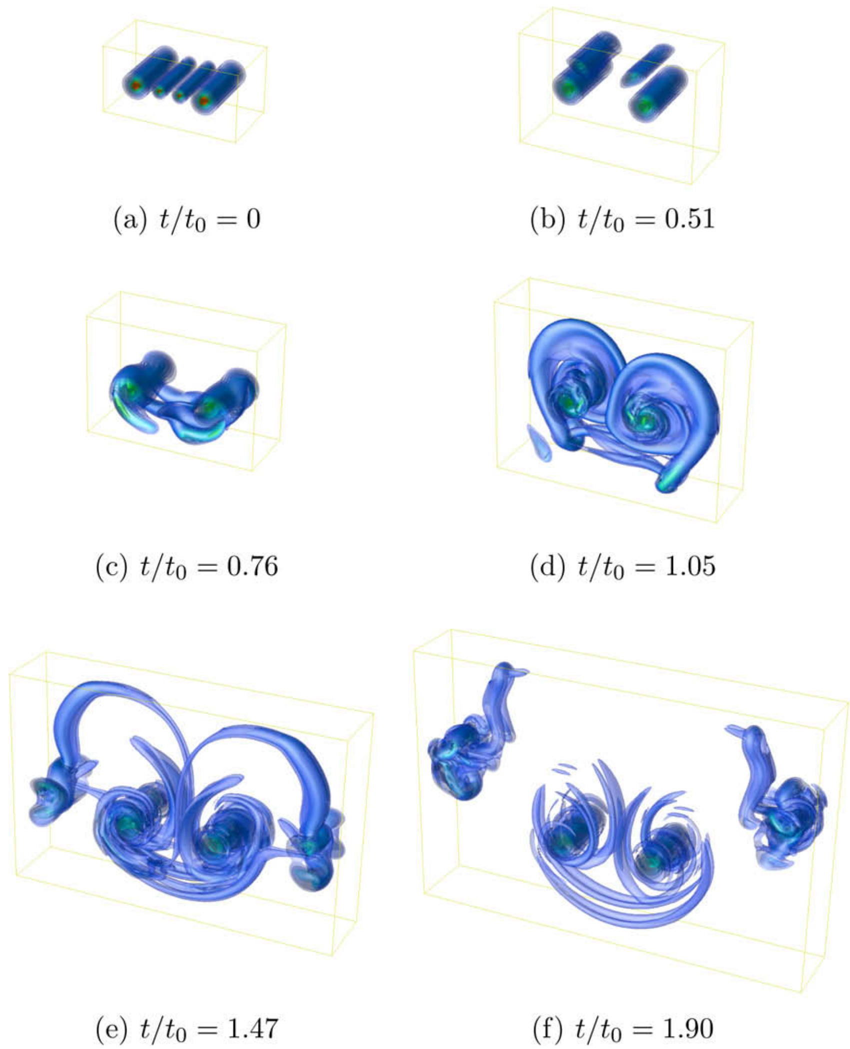

Fig. 1. Counter-rotating vortex pairs: isosurfaces of vorticity norm, from opaque red to transparent blue, $|\boldsymbol{\omega}| = 1/2, 1/4, 1/8, 1/16, 1/32, 1/64|\boldsymbol{\omega}|^{t=0}_{\max}$ and computational domain. (For interpretation of the references in color in this figure legend, the reader is referred to the web version of this article.)

(2) in space: the present approach does not preclude the use of embedded coarser grids (as in [3]) in order to alleviate the truncation issue. In fact the combination of the present method with the embedded coarser grids can lead to significant computational savings for simulations of vortical flows.

3. Results

We assess our periodic–unbounded solver in conjunction with a vortex particle method on a problem of trailing vortices. This problem has been a benchmark in several works [1,11] and involves counter-rotating vortices that undergo a medium-wavelength instability [7]. In this setup, the secondary pair which accounts for outboard wing loading or a stabilizer, has a span $b_2 = 0.3b_1$ and a circulation $\Gamma_2 = -0.3\Gamma_1$. We refer to [11] for a full description of the initial condition.

In Fig. 1, we show the evolution of the vortex structures through the instability along with the computational domain. In this simulation, a threshold value $3.5 \times 10^{-4}|\omega|_{\max}(t)$ was used. This led to a domain resizing every few tens or even hundreds of time steps, a manageable frequency. As a result, the computational domain went from $128 \times 256 \times 128$ to $128 \times 896 \times 584$, efficiently tracking and adapting to the growing support of vorticity.

We illustrate the convergence of the method and the elliptic solver with $N_x = 64$, 128 and 256 points in the periodic direction. The time histories of enstrophy $\epsilon = \int \omega \cdot \omega dV$ in Fig. 2 indicate that the coarse mesh smears the initially sharp vortex tubes markedly. In Fig. 3, we compare the vorticity structures at the approximate time of peak dissipation $(t = 1)$ for the three resolutions. The choice of high vorticity values emphasizes the effects of numerical dissipation. As expected, the coarse mesh cannot capture the high vorticity in the stretched structures. Furthermore, the vortex structures which are advected and deformed in the vicinity of the primary core trail behind those of the high resolution meshes ($N_x = 128$ and 256).

Fig. 4 shows the evolution of the first energy modes

$$E_{k_x}(t) = \iint \tilde{\mathbf{u}}(k_x, y, z) \cdot \tilde{\mathbf{u}}^*(k_x, y, z)\, dy\, dz \tag{15}$$

$$= \iint \frac{1}{2}(\tilde{\boldsymbol{\psi}} \cdot \tilde{\boldsymbol{\omega}}^* + \tilde{\boldsymbol{\psi}}^* \cdot \tilde{\boldsymbol{\omega}})\, dy\, dz. \tag{16}$$

The second identity is obtained through vector analysis and is conveniently evaluated in wave space through Parseval's identity. The three resolutions are in excellent agreement over the linear phase of the instability; the coarsest resolution starts to deviate from the others in the features of the mode $(k_x = 2)$ at the end of the linear regime $(t/t_0 = 0.6)$.

If we measure the growth rate σ_M as

$$E_1(t) \sim E_1(0)e^{2\sigma_M t} \tag{17}$$

we obtain $\sigma_M \simeq 13.4$ for $t \in [0.15, 0.67]$. Our value is consistent with the value of 14.5 from the results of [11], which were obtained with a hybrid FMM-grid solver. The slightly larger growth rate is due to the fact that the simulation of [11] is inviscid and rather uses a hyper-viscosity model.

The simulations presented in this section were run on the Cray XT5 at the Swiss Supercomputing Center (CSCS). The case $N_x = 64$ ran on 128 cores for 1.4 wallclock-hours; the case $N_x = 128$ used 256 cores for 4.4 h; the case $N_x = 256$ used 1024 cores for 9.4 h.

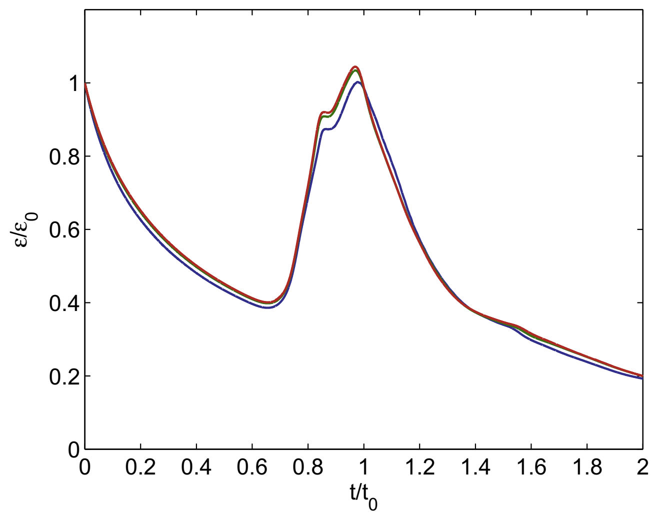

Fig. 2. Counter-rotating vortex pairs: evolution of the enstrophy for grid sizes $N_x = 64$ (blue), 128 (green) and 256 (red). (For interpretation of the references in color in this figure legend, the reader is referred to the web version of this article.)

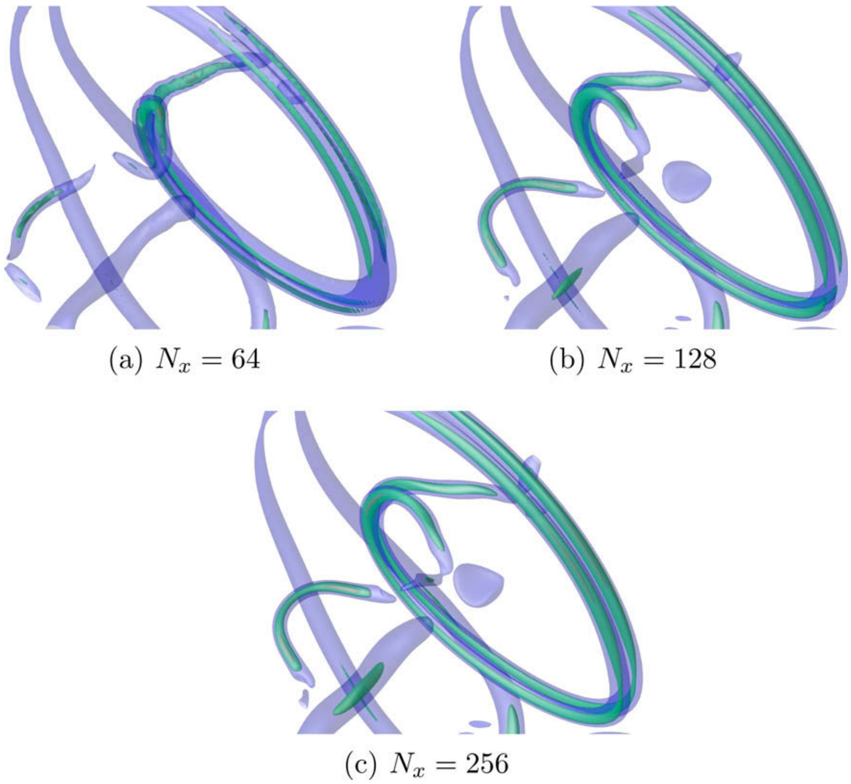

Fig. 3. Counter-rotating vortex pairs: isosurfaces of vorticity norm in the reconnection region and primary vortex core, from opaque red to transparent blue, $|\boldsymbol{\omega}| = 1/2, 3/8, 1/4|\omega|_{\max}^{t=0}$. (For interpretation of the references in color in this figure legend, the reader is referred to the web version of this article.)

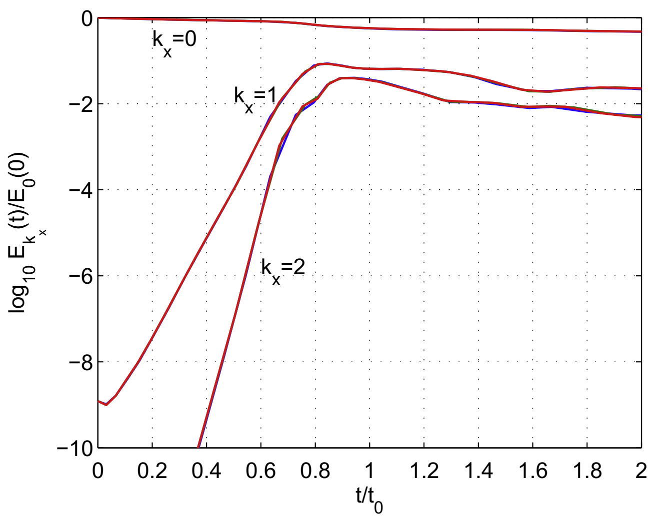

Fig. 4. Counter-rotating vortices: evolution of the longitudinal energy modes for grid sizes $N_x = 64$ (blue), 128 (green) and 256 (red). (For interpretation of the references in color in this figure legend, the reader is referred to the web version of this article.)

4. Conclusions

We have introduced an extension of the fast convolution technique of Hockney and Eastwood to the solution of Helmholtz and Poisson equations in periodic–unbounded domains. This technique can be readily adapted to any Fourier-based solver, even parallel. When compared to the full periodic solver, the present technique incurs an overhead factor larger than two in three dimensions. This assumes however meshes of equal sizes; the full periodic solver will have to use a large grid to alleviate the effect of periodic images.

We have employed this technique in conjunction with a three-dimensional vortex particle method in the study of a benchmark vortex instability. The method was implemented within the parallel framework of the Parallel Particle Mesh library [10]; it displays convergence and agrees with results obtained with Fast Multipole Methods.

Ongoing efforts include performance comparisons with other approaches and the application to the massively parallel simulation of vortical flows. The combination of the present unbounded Poisson solvers and the coarsening and embedded grid techniques as introduced in [3] briefly discussed in Section 2.4 are areas of future work.

Acknowledgments

We wish to acknowledge several helpful discussions with Prof. Tim Colonius (Caltech). We gratefully acknowledge the computational time provided by the Swiss Supercomputing Center (CSCS).

References

[1] P. Chatelain, A. Curioni, M. Bergdorf, D. Rossinelli, W. Andreoni, P. Koumoutsakos, Billion vortex particle direct numerical simulations of aircraft wakes, Computer Methods in Applied Mechanics and Engineering 197 (13) (2008) 1296–1304.
[2] H.W. Cheng, W.Y. Crutchfield, Z. Gimbutas, L.F. Greengard, J.F. Ethridge, J.F. Huang, V. Rokhlin, N. Yarvin, J.S. Zhao, A wideband fast multipole method for the Helmholtz equation in three dimensions, Journal of Computational Physics 216 (1) (2006) 300–325.
[3] T. Colonius, K. Taira, A fast immersed boundary method using a nullspace approach and multi-domain far-field boundary conditions, Computer Methods in Applied Mechanics and Engineering 197 (25–28) (2008) 2131–2146.
[4] L. Greengard, V. Rokhlin, A fast algorithm for particle simulations, Journal of Computational Physics 73 (1987) 325–348.
[5] R. Hockney, J. Eastwood, Computer Simulation using Particles, Institute of Physics Publishing, 1988.
[6] P. Koumoutsakos, Multiscale flow simulations using particles, Annual Review of Fluid Mechanics 37 (2005) 457–487.
[7] J.M. Ortega, Ö. Savas, Rapidly growing instability mode in trailing multiple-vortex wakes, AIAA Journal 39 (4) (2001) 750–754.
[8] D.S. Pradeep, F. Hussain, Effects of boundary condition in numerical simulations of vortex dynamics, Journal of Fluid Mechanics 516 (2004) 115–124.
[9] S.C. Rennich, S.K. Lele, Numerical method for incompressible vortical flows with two unbounded directions, Journal of Computational Physics 137 (1) (1997) 101–129.
[10] I.F. Sbalzarini, J.H. Walther, M. Bergdorf, S.E. Hieber, E.M. Kotsalis, P. Koumoutsakos, PPM a highly efficient parallel particle mesh library for the simulation of continuum systems, Journal of Computational Physics 215 (2006) 566–588.
[11] G. Winckelmans, R. Cocle, L. Dufresne, R. Capart, Vortex methods and their application to trailing wake vortex simulations, Comptes Rendus Physique 6 (4–5) (2005) 467–486.